Tuning surface interactions on MgFe2O4 nanoparticles to induce interfacial hyperactivation in Candida rugosa lipase immobilization

Andrés H. Morales, Johan S. Hero, Ana E. Ledesma, M. Alejandra Martínez, María C. Navarro, María I. Gómez, Cintia M. Romero

PII: S0141-8130(23)03511-0

DOI: https://doi.org/10.1016/j.ijbiomac.2023.126615

Reference: BIOMAC 126615

To appear in: *International Journal of Biological Macromolecules*

Received date: 22 May 2023

Revised date: 15 August 2023

Accepted date: 28 August 2023

Please cite this article as: A.H. Morales, J.S. Hero, A.E. Ledesma, et al., Tuning surface interactions on MgFe2O4 nanoparticles to induce interfacial hyperactivation in Candida rugosa lipase immobilization, *International Journal of Biological Macromolecules* (2023), https://doi.org/10.1016/j.ijbiomac.2023.126615

Tuning surface interactions on $MgFe_2O_4$ nanoparticles to induce interfacial hyperactivation in *Candida rugosa* lipase immobilization

Andrés H. Morales[a*], Johan S. Hero[a], Ana E. Ledesma[b], M. Alejandra Martínez[a,c], María C. Navarro[d], María I. Gómez[d], Cintia M. Romero[a,d*]

[a]*Planta Piloto de Procesos Industriales Microbiológicos PROIMI-CONICET, Av. Belgrano y Pasaje Caseros, T4001 MVB, Tucumán*

[b]*Centro de Investigación en Biofísica Aplicada y Alimentos (CIBAAL-UNSE-CONICET), Departamento Académico de Química, Facultad de Ciencias Exactas y Tecnológicas, Universidad Nacional de Santiago del Estero, Av. Belgrano Sur 1912, (4200) Santiago del Estero, Argetnina.*

[c]*Facultad de Ciencias Exactas yTecnología, UNT. Av. Independencia 1800, San Miguel de Tucumán, 4000, Argentina.*

[d]*Facultad de Bioquímica, Química y Farmacia UNT. Chacabuco 461, T4000IL – San Miguel de Tucumán, Argentina.*

*Corresponding Authors:

Cintia Mariana Romero. PROIMI, PROIMI-CONICET, Av. Belgrano y Pasaje Caseros, T4001 MVB, Tucumán Fac. Bioq., Qca. y Farmacia (UNT), Ayacucho 461, 4000, Tucumán, Argentina. Telephone +54-0381-4344888. Fax: +54-0381-434488. E-mail: cinromero78@gmail.com

Andrés Hernán Morales. PROIMI, PROIMI-CONICET, Av. Belgrano y Pasaje Caseros, T4001 MVB, San Miguel de Tucumán, Provincia de Tucumán, Argentina. Telephone +54-0381-4344888. Fax: +54-0381-434488. E-mail: andymorales_2006@hotmail.com

Abstract

Lipase adsorption on solid supports can be mediated by a precise balance of electrostatic and hydrophobic interactions. A suitable fine-tuning could allow the immobilized enzyme to display high catalytic activity. The objective of this work was to investigate how pH and ionic strength fluctuations affected protein-support interactions during immobilization via physical adsorption of a *Candida rugosa* lipase (CRL) on $MgFe_2O_5$. The highest amount of immobilized protein (IP) was measured at pH 4, and an ionic strength of 90 mM. However, these immobilization conditions did not register the highest hydrolytic activity (HA) in the biocatalyst (CRLa@$MgFe_2O_4$), finding the best values also at acidic pH but with a slight shift towards higher values of ionic strength around 110 m*M*. These findings were confirmed when the adsorption isotherms were examined under different immobilization conditions so that the maximum measurements of IP did not coincide with that of HA. Furthermore, when the recovered activity was examined, a strong interfacial hyperactivation of the lipase was detected towards acidic pH and highly charged surrounding environments. Spectroscopic studies, as well as *in silico* molecular docking analyses, revealed a considerable involvement of surface hydrophobic protein-carrier interactions, with aromatic aminoacids, especially phenylalanine residues, playing an important role. In light of these findings, this study significantly contributes to the body of knowledge and a better understanding of the factors that influence the lipase immobilization process on magnetic inorganic oxide nanoparticle surfaces.

Keywords: ionic strength; lipase immobilization; interfacial hyperactivation; adsorption; hydrophobic interactions.

1. Introduction

Enzyme immobilization is the process that involves both a conformational change and a complete or partial restriction of the degrees of freedom of biocatalyst movement, because of its binding or anchoring to physical support. The biocatalyst must retain its entire or partial catalytic activity after the immobilization process to produce an active and efficient system. In this line, enzyme immobilization onto solid supports could allow easy reuse of these biocatalysts, whose production and purification are usually expensive [1].

The enzyme simple adsorption on solid substrates methodology has been the easiest, cheapest, and simplest to implement [2]. During enzyme confinement in a solid surface, a solid-liquid interface forms a microenvironment relative to the surrounding aqueous solution that can affect protein structure and activity [3]. In addition, the solid surface exerts an electrostatic field that could affect the behavior of the solvent molecules, buffer salts, substrates, products, and even the same enzymes [4].

Among the most widely used enzymes at an industrial level, the lipases (triacylglycerol ester hydrolases, EC 3.1.1.3) are enzymes that catalyze the hydrolysis of ester bonds present in acylglycerols [5]. These enzymes display their full catalytic capability linked to lipid-water interfaces; as a result, when they contact with the aforementioned interface, they produce an activity greater than that shown in the aqueous phase, a process known as interfacial activation. This process is mediated through a conformational change involving a chain of hydrophobic amino acids (lid) that can cover the active site of the enzyme (closed conformation) or expose it (open conformation) [6]. Considering this behavior, electrostatic and hydrophobic interactions drive protein-support interaction in the lipase immobilization process [7]. These enzymes tend to increase their relative activity when they are selectively adsorbed on hydrophobic supports since they can recognize surfaces similar to their natural substrates, and thus undergo interfacial activation during immobilization [8,9]. However, the hydrophobicity of the support is not a dominant parameter in the lipase immobilization efficiency; since the polarity of the enzyme microenvironment has a strong impact on the protein-support interaction [10].

In this sense, the lipase adsorption phenomenon to different supports is strongly determined by the pH and the ionic strength of the reaction medium [11]. The pH

determines the nature of the charges present in the support and in the immobilized protein, which will depend mainly on its isoelectric point. In this way, pH modification influences the formation of electrostatic-type interactions and lipase-support hydrogen bonds [12]. Instead, variations in ionic strength impact the surface ionic bacchants of proteins and supports by exerting a shielding effect through the ions present in the solution. [13]. As a result of the ion competition, increases in ionic strength weaken electrostatic interactions between proteins and the support, favoring the formation of hydrophobic contacts. The latter is mostly owing to the necessity to stabilize the most hydrophobic portions of the protein that are exposed as a result of protein dehydration, as the surrounding water molecules are involved in the hydration of salt ions [14].

Magnetic inorganic particles constitute one of the supports most used for enzyme immobilization since they provide some advantages such as small particle size, super-paramagnetism, and a large specific surface area [1]. Among the different magnetic particles, mixed iron oxide nanoparticles (IONPs) have gained a lot of attention for their efficient support properties and easy recovery with the assistance of a magnetic field [15]. These compounds are featured by the presence of multiple surface ionizable hydroxyl groups, which are widely employed to anchor new chemical groups. Indeed, it is usual to functionalize IONPs for enzymatic immobilization using organic and inorganic chemicals to avoid nanoparticle aggregation, limit interactions with system components, and add chemical groups to facilitate enzyme binding. This allows for the creation of a wide range of protocols and methodologies for biocatalytic systems [16–19]. However, research into direct interactions between "naked" IONPs and immobilized enzymes is currently incipient and little explored [20,21].

The aim of this work was the study of support-protein interactions in the adsorption of *Candida rugosa* lipase (CRL) on $MgFe_2O_4$ nanoparticles. This novel support is a cubic spinel ferrite nanoparticle, synthesized by our work group through a thermal decomposition process of an inorganic precursor. It was previously used as a support for lipase immobilization through covalent bonds demonstrating utility in the manufacture of biodiesel [22] and the enrichment of fish oil polyunsaturated fatty acids content [23]. Besides, this support was recently used in the immobilization by adsorption of lipase

enzyme aggregates (CLEAs) [24]. Following this line of work, the present paper strongly focuses on the study of protein-support surface interactions to improve catalytic activity by controlling the environment involved in the immobilization process. The influence of pH and ionic strength on this was explored using a response surface methodology, which, unlike "one factor at a time" studies, provides for a full evaluation of the interaction between the variables under consideration. Although these statistical designs are generally utilized as response optimizers, our work aims to use this tool as a key axis of research to deep inside the interactions that occur between the enzyme and the support during immobilization.

2. Materials and Method

2.1. Chemicals and reagents

CRL (LT1754), bovine albumin (BSA), Coomassie Blue G-250, p-nitrophenylpalmitate (p-NPP), and pentacyanonitrosil ferrate salts were purchased from *Sigma-Aldrich*. All organic solvents (*Sintorgan S.A.)* were used without further purification. Chemical substances intended for buffer preparation (Na_2HPO_4, NaH_2PO_4, citric acid, sodium citrate, $NaHCO_3$, and H_2CO_3) were purchased from *Cicarelli*.

2.2. Lipase immobilization

2.2.1. Support synthesis

The synthesis of $MgFe_2O_4$ used as support for lipase immobilization was carried out by thermal decomposition of $Mg[Fe(CN)_5NO]\cdot 4H_2O$ [25]. Platinum crucibles with the solid inorganic complex were placed in a muffle furnace (Furnace DM 40, Zhemack technical) with programmed temperature ramps, for 5 h until reaching 650ºC, and then allowed to stand for 12 h at room temperature. In the end, the solid obtained corresponded to $MgFe_2O_4$ or magnesium ferrite. The synthesis of the precursor inorganic complexes as well as the study of the thermal decomposition until obtaining the mixed oxide has been previously studied in a work carried out by our group [22].

2.2.2. Response Surface Methodology

Using the DesignExpert®11 software, a response surface methodology (RSM) was proposed using a central composite design (CCD), to study the effect of pH and ionic strength on the immobilization of *C. rugosa* lipase onto $MgFe_2O_4$ by physical adsorption. The responses used to evaluate the design were: immobilized protein, hydrolytic activity, specific activity, Gibbs free energy, immobilization yield, and recovered activity. Two levels (+1 and -1) were selected for each factor, plus a central point (0) with pH values of 4, 6, and 8, while for the ionic strength of 50, 100, and 150 mM, obtaining a total of 20 trials with duplicates included (**Supplementary Material - Table S1**). For the adjustment of the different conditions of pH and ionic strength, the following buffers with the appropriate molarity were used: citrate for pHs 3 and 4; phosphate for pHs 6 and 8, and carbonate for pHs higher than 8. The general immobilization protocol to carry out the process was at 25ºC with constant agitation for 18 h. Additionally, the initial protein concentration in all assays was 35 µg/mL, always maintaining a 1:9 (m/v) ratio of support: enzyme solution. The immobilized biocatalysts obtained at the end of the process (CRLa@$MgFe_2O_4$) were recovered magnetically and washed twice with distilled water.

2.2.3. Protein determinations

Lipase activity was measured using p-nitrophenol palmitate (p-NPP) as substrate [26]. Free (100 µL) or immobilized lipase (0.005 g) was dissolved to a final volume of 1 mL in the following reaction mixture: 100 mM pH 7 phosphate buffer, 0.01% w/v gum Arabic, 0.4% w/v Triton X-100, and 1 mM p-NPP. This was gently stirred at 37°C for 10 minutes and then was centrifuged for 30 s (10,000 rpm) to separate the supernatant from the solid in the immobilized enzyme. The p-nitrophenol (p-NP) released as a result of enzymatic hydrolysis was quantified spectrophotometrically at 405 nm. One unit of international enzyme activity (IU) was defined as the amount of biocatalyst that released 1 µmol of p-NP per minute under standard conditions described for the assay.

Bradford's methodology [27] was used for protein quantification using bovine serum albumin (fraction V) as standard.

2.2.4. Immobilization parameters

The amount of immobilized protein (**IP**) on $MgFe_2O_4$ (mg protein/mg support) was calculated according to the following equation:

$$IP = \frac{V_{enz}(C_0 - C_f)}{m}$$

Where V_{enz} is the volume of the enzymatic solution in mL, C_0 is the initial protein concentration (mg/mL), C_f is the residual concentration of protein in solution after the immobilization process (mg/mL) and m is the mass of the support (mg).

The specific activity (**SA**) (IU/mg protein) was calculated as the ratio between the lipolytic activity in the biocatalyst (IU/mg protein support) (**HA**) and the amount of immobilized protein (**IP**).

For its part, the Gibbs free energy (kJ/mol) was determined according to the following equation:

$$\Delta G = -RT \ln K_c \;\therefore\; K_c = \frac{IP}{C_e}$$

With R as the universal gas constant (8.314×10^{-3} kJ/mol.K), T is the absolute temperature (298.15 K) and K_c is the equilibrium constant. K_c was determined as the ratio between the amount of protein immobilized protein (***IP***) and residual protein concentration (C_e) at equilibrium.

The immobilization yield (**IY**) was determined according to the following equation:

$$IY(\%) = \left(\frac{EA_0 - EA_f}{EA_0}\right) x\ 100$$

Where EA_0 and EA_f are the enzymatic activities of the solution before and after enzyme immobilization (IU/mL), respectively.

Finally, the recovered activity (**RA**) expressed as a percentage was calculated as follows:

$$RA(\%) = \frac{HA}{IU_i\ x\ IY}\ x\ 100$$

Where ***HA*** is the hydrolytic activity of the biocatalyst (IU/mg support) y IU_i is the activity of the soluble enzyme before immobilization (IU/mg support) and ***IY*** is the immobilized yield described above.

2.2.5. Stability tests

Comparative stability studies were carried out between the free and immobilized lipase as a function of temperature, pH, and different organic solvents. The temperature range evaluated was 30-80ºC and the samples were prepared in 50 mM pH 7 phosphate buffer. The pH was evaluated from 2 to 10 and the samples were left to stand at room temperature (near 25°C). Finally, the samples were exposed at 25ºC to the following organic solvents (50% v/v): methanol, ethanol, propanol, butanol, ethyl acetate, acetone, and hexane. The incubation times of all the samples under different conditions was one hour. After this period, the residual activity of the biocatalyst was measured taking into account the conditions detailed above (***Section 2.2.3.***). In all cases, the residual activity observed in the different catalytic systems was calculated considering 100% of the enzymatic activity determined under standard conditions.

2.3. Physic-Chemical characterization

2.3.1. Adsorption isotherms

The effect of initial protein loading on the immobilization process was examined. The adsorption conditions in terms of pH and ionic strength were set based on the results obtained in the CCD, while the other factors were kept as those described above (***Section 2.2.2.***). The experimental data obtained from the protein adsorption equilibria for the different conditions were fitted to non-linear models for the Langmuir (**Eq. 1**) and Freundlich (**Eq. 2**) isotherms whose equations are described below:

$$q_e = \frac{q_{max}.C_e}{K_L + C_e} \qquad \textbf{Eq. 1}$$

$$q_e = K_F.C_e^{\frac{1}{n}} \qquad \textbf{Eq. 2}$$

Where q_e is the adsorption capacity at equilibrium (mg protein/mg support), C_e is the residual mass of protein per unit volume in the lipase solution (mg protein/mL), q_{max} is the maximum adsorption capacity of the support, K_L is the Langmuir constant which is related to the adsorption energy (mL/mg protein), K_F is the Freundlich isotherm constant (mL/mg protein) and n is the Freundlich exponent (dimensionless).

Previous equations were also adapted to describe the equilibria in terms of the hydrolytic activities measured before and after the immobilization process:

$$A_e = \frac{A_{max}.a_e}{K_L + a_e} \qquad \textbf{Eq. 3}$$

$$A_e = K_F . a_e^{\frac{1}{n}} \qquad \textbf{Eq. 4}$$

Where A_e is the hydrolytic activity recorded on the support at equilibrium (IU/mg support), a_e is defined as the residual activity per mg of support in solution after immobilization (IU/mg support), q_{max} is the maximum activity hydrolytic that could be found in the support according to the model (IU/mg support).

The choice of the type of isotherm that best describes the adsorption process on both supports was based on the determination of the correlation coefficients (R^2) from the non-linear regressions in both models.

2.3.2. Surface charge

The measurements of surface charge by ζ potential of the nanoparticles studied were carried out using a DLS SZ-100 Horiba. Dispersions of the nanoparticles (0.5 mg/mL) were made in buffer solutions of different pH and ionic strengths. Before taking the measurements, all the dispersions were sonicated for 10 minutes to avoid the formation of aggregates. The detection angle was 173° and for each of the samples, at least 30 measurements were made in a period of 30 s.

2.3.3. Spectroscopical analysis

Attenuated Total Reflectance Fourier transform infrared (ATR-FTIR) spectra were recorded for the different samples on a Thermo Nicolet 6700 spectrometer equipped with a DTGS KBr detector, and KBr beam splitter. 1 mg of each sample placed on a crystal was and the measurements were obtained using an AMTIR crystal element in a horizontal ATR cell (Thermo Nicolet, Inc.). FTIR spectra were processed by OPUS 7.0 software.

The Raman spectra for the different samples were measured using a Raman DXR Microscope (Thermo Fisher Scientific). Data were collected using a solid-state laser from a 532-nm iodine pump using a power of 10 mW (spectral resolution of 5 cm^{-1}). A confocal slit opening of 50 µm and a 40X objective was used for data collection. To achieve a high enough signal-to-noise ratio, 80 laser exposures were made in a time of 6 s that were accumulated for all samples.

2.4. *In silico* analysis

Molecular docking studies were carried out to study the interaction between *C. rugosa* lipase and the $MgFe_2O_4$. The crystal structure of this enzyme in its open conformation was obtained from the Protein Data Bank (PDB: 1CRL) [28], and its visualization was performed using the UCFS Chimera V1.13 software [29]. On the other hand, the structures of the oxides were generated and optimized using the Gaussian®16 program and the Crystallography Open Database. They consisted of three-dimensional orthorhombic and cubic networks obtained by doubling the unit cell along one of the crystal planes. Protein-support docking studies were carried out using AutoDock 4.2, taking the oxide meshes as enzyme ligands.

2.5. Statistical analysis

All the samples and assays carried out in this work were performed in triplicate and the results are reported as the mean and its standard deviation (SD). The comparative analyses were carried out using the Minitab19® software through a Tukey`s test ($\alpha = 0.05$).

3. Results and Discussion

3.1. Effect of pH and ionic strength on the immobilization process

Protein immobilization by adsorption on support would be mediated through a delicate balance between electrostatic and hydrophobic interactions. Their appropriate fine-tuning would allow the exhibition of high catalytic activities in the immobilized enzyme [30]. In this sense, the pH would play a crucial role by controlling the ionization of the acid and base groups in the protein. On the other hand, the degree of dissociation of these groups would also be directly influenced by the local electrostatic field near the surface, which would be given by the ionic strength of the surrounding solution [31]. Taking this into account, in this work the pH and the ionic strength were taken as variables to study the CRL immobilization by adsorption on the mixed oxide $MgFe_2O_4$ using an RSM. Through a central composite design (CCD) the statistical parameters calculated based on the experimental data for each response evaluated are summarized in **Table 1** and will be described in detail in the following sections. The data matrix obtained for all the responses of the design in all the runs is detailed in **Table S1** (**Supplemental Material**). All of the statistical estimators ensured strong reproducibility, reliability, and homogeneity in the

measured data, as well as an agreement between the practical values and those predicted by the generated models (**Table 1** and **Supplementary Material - Table S2**). Finally, the responses were fitted to second-order polynomial equations using the significant variables and interactions, which are outlined in the **Supplementary Material**.

3.1.1. Factor influence on immobilized protein (IP) and hydrolytic activity (HA)

Based on the surface graph in **Figure 1A**, the highest measurements of **IP** were recorded at pH 4 and 90 mM of ionic strength. When we compare these results with those obtained with **HA** as a response to the design (**Figure 1B**), the highest **HA** values were also recorded at acid pH but, unlike the **IP**, the maximum peak measured had a slight shift towards higher values of ionic strength near to 110 mM. Taking a more general viewpoint, we can observe that the highest **IP** values were recorded at pH 4 in the ionic strength range of 50 to 120 mM, whereas the greatest **HA**s were in the region of 90 to 150 mM. In this way, the conditions that maximized the amount of **IP** did not coincide with the maximum **HA** values. Similar results were reported by Collu et al. [32] when evaluating the immobilization of *Pseudomonas fluorescens* lipase against different ionic strengths.

Physical adsorption of enzymes typically involves electrostatic and hydrophobic interactions that contribute in different proportions, resulting in a multipoint union between the protein and the support. Electrostatic interactions are favoured during immobilization at low ionic strengths because competition between the ions in the medium and the ionic groups on the enzyme and support surfaces is reduced [33,34]. Meanwhile, in high-ionic-strength settings, the hydrophobic portions of the protein are exposed due to dehydration caused by the shielding of surface charges by salt ions [35,36]. Thus, under these conditions, hydrophobic protein-carrier interactions would be favoured. Given the charged nature of the surface of $MgFe_2O_4$, ion exchange is likely to play a key role in protein-carrier interaction. As a result, increasing ionic strength reduces the number of electrostatic contact locations with the enzyme. Keeping this in mind, our findings suggest that a higher proportion of electrostatic interactions mediating lipase binding at low ionic strengths would allow better **IP** values to be obtained. At higher ionic strength, however, we found a decrease in **IP** measurements as the participation of hydrophobic contacts between the enzyme and the oxide increased.

The best **IP** and **HA** values observed at pH 4 in our experiments could be attributed to the enzyme being immobilized in a more favourable spatial orientation, which could improve its catalytic performance. Recently, Silva Cavalcanti et al. examined the immobilization of *Thermomyces lanuginosus* lipase on "naked" iron oxide nanoparticles via physical adsorption [20]. These authors performed an *in-silico* study of the enzyme's surface charge at pH 4 and 8, indicating that at acidic pH, protein-support binding would be preferred in regions opposing the enzyme's catalytic site. The experimental support for this idea led them to believe that these conditions allowed for directed immobilization of the lipase, exposing its active region. CRL has an isoelectric point near 4.5 [37,38], so, at acid pH, it has a slightly positive net charge. The occurrence of hydrophobic interactions with the support that allows an interfacial activation is more feasible as we approach the isoelectric point of the lipase and this could be reflected in the highest values of **IP** and **HA** obtained at an acid pH [39]. This behaviour was also previously reported by Alves et al. [40] and Sarno and Iuliano [41] who found that in the immobilization of *T. lanuginosus* lipase the best records for the amount of protein adsorbed was at pH 5, near to its isoelectric point (4.4). On the other hand, when the pH increases, it would be expected that the contribution from electrostatic interactions would begin to unfavourably affect the enzyme's attachment. This is because, when we are over the isoelectric point, the lipase gets a net negative charge like the support surface, leading to electrostatic repulsion [42]. This can be seen in our results, where the lowest **IP** and **HA** values were obtained at pH 8.

Traditionally, acidic pH and low ionic strength are the most used conditions to maximize lipase immobilization yields due to two main reasons: the conformational equilibrium of the lipase is shifted towards its open form and the formation of lipase-lipase dimers is reduced [11,43]. Our studies reveal that these parameters coincided to boost the amount of **IP** but not **HA**. One possible explanation for the reduced activity levels seen at low ionic strengths is a high density of adsorbed enzyme per support surface, which causes diffusional limitations [44]. Although a rise in ionic strength reduces the fraction of immobilized lipases in their open state, they may experience interfacial hyperactivation due to increased exposure of their hydrophobic residues near the enzyme's active site. Moreover, at high ionic strength, the exposure of the lipase's hydrophobic areas also induces protein dimers formation, which would be detrimental to **HA**. Based on our

findings, this phenomenon may have been relevant at very high ionic strengths of 150 mM, when a decline in **HA** was observed.

3.1.2. Factor influence on specific activity (SA) and Gibbs free energy (ΔG)

In the case of **SA**, the lowest computed values were obtained mainly at acidic pH (**Figure 1C**), which may imply that a proportion of proteins immobilized are catalytically inactive. As previously stated, this could be either due to the formation of dimers/protein aggregates or the high density of enzyme adsorbed on the surface of the oxide. On the other hand, **SA** values varied greatly at pH 8, observing the highest one at 100 mM. Despite this, the lowest values of **IP** and **HA** were obtained under these conditions, as seen in the aforementioned results.

When analyzing the design taking the Gibbs free energy as a response (**Figure 1D**) this parameter took negative values in all the conditions evaluated, demonstrating that the adsorption process occurred spontaneously. According to the literature, **ΔG** values in the range of 0 to -20 kJ/mol correspond to a physisorption bonding process; while values below -40 kJ/mol would indicate a bonding process by chemisorption [45]. In our experimental data, the **ΔG** values ranged between -11.40 and -24.08 kJ/mol, suggesting that physical forces guided the lipase interaction on $MgFe_2O_4$. As expected, the most negative values of **ΔG** coincide with those points where the highest **IP** was recorded, where the adsorption equilibrium was more shifted to lipase adsorption, resulting in a more spontaneous process.

In line with the analysis of **ΔG**, adsorption isotherms at 25ºC were performed to study the relationship between the concentration of lipase adsorbed on $MgFe_2O_4$ and its residual concentration in the aqueous phase at equilibrium [46]. Two conditions were optimized from the models generated in the CCD: maximizing **IP** or **HA**. The amount of protein at which the system becomes saturated was determined and the experimental data of the protein adsorption and activity isotherms were adjusted to the non-linear models of Langmuir or Freundlich (**Figure 2**). **Table 2** details the conditions given by the CCD to obtain the maximum values of **IP** and **HA**, as well as the theoretical value predicted for these responses, their desirability, and the practical value obtained under the design conditions.

The protein isotherms reflected a high enzyme-support affinity due to the sharp increase observed at low concentrations and then stabilize at higher ones (**Figure 2. A1** and **A2**). In all cases, the data fitted the Langmuir model better than Freundlich (**Table 2**) which is based on the formation of a molecular layer of adsorbate that interacts with the surface of the adsorbent with all adsorption points with the same binding energy [47]. In general, the Langmuir adsorption model is usually the most common by which proteins are adsorbed on different supports, with previous reports for the immobilization of lipases by physical adsorption on oxides such as Fe_3O_4 [48], SiO_2 [16,49] or CuO [50].

One of the most important data provided by the fit to a Langmuir model is the maximum amount of protein that the support is capable of adsorbing (q_{max}). Under the conditions where the **IP** was maximized, $MgFe_2O_4$ would be capable of adsorbing up to 3.888 mg protein/mg support, while when the conditions were set to maximize the **HA**, the model predicted a 3.197 mg protein/mg support adsorption (**Table 2**). In turn, we can notice how these maximum estimated values after adjusting the experimental data to the Langmuir model were close to those predicted by the model generated from the CCD, and the practical values obtained experimentally in standard tests.

When analyzing the activity isotherms (**Figure 2. B1** and **B2**) and the parameters determined for the adjustment to each model (**Table 2**), it was observed that these data also fitted better for a Langmuir model. In the conditions to maximize **HA**, values near 76 U/mg support were recorded. It should also be noted that the conditions that enhance **HA** consider ionic strengths greater than 100 mM, where hydrophobic interactions between the protein and the support would be maximized. These experimental observations once again confirm that there was no correlation between the maximum **IP** and the maximum **HA**.

3.1.3. Factor influence on immobilization yield (IY) and recovery activity (RA)

The **IY** reflects the percentage of theoretical activity that would be retained on the support based on the drop-in activity measured in the supernatant before and after the immobilization process. As can be seen in the surface graph in **Figure 1E**, the behavior of this response showed a strong dependence on both the pH and the ionic strength and their interaction ($p < 0.05$; **Table 1**). The highest **IY** was recorded at the extreme points of the statistical environment analyzed, showing a curvature towards minimum values of the

response when working in intermediate conditions of pH and ionic strength, reflecting the statistical significance that the quadratic terms had in the model (**Table 1**). It was interesting to observe how a high **IY** was obtained at pH 8, comparable to those recorded at pH 4, even though, as previously observed, their **IP** and **HA** records were considerably lower. This may be because, during the adsorption of the enzyme to the support at pH 8, conformational changes would produce in the lipase, altering its stability and compromising its catalytic capacity. As the results described above indicate, only a small amount of protein was adsorbed under alkaline conditions. In previous works carried out by our working group, we observed that the stability of the lipase of *C. rugosa* decreases rapidly at alkaline pH [22] so it is likely that a proportion of lipases that remained in the supernatant after immobilization was not catalytically active, which would lead to higher **IY** values, thus overestimating the real value. At pH 4, we can see how the **IY** reduced as the ionic strength increased. These findings are congruent with the **IP** measurements (**Figure 1A**), which revealed that the lowest levels of adsorbed protein were seen at high ionic strengths. Thus, the **IY** values at acidic pH are mostly explained by an enzyme adsorption process on the support. When these results were compared to the **HA** values at pH 4 (**Figure 1B**), the lowest **IY** coincided with the greatest **HA** values, which could suggest activation of the immobilized lipase.

On the other hand, **RA** reflects the percentage of the activity recorded in the adsorbed enzyme concerning that is theoretically lost in the enzymatic solution used for immobilization [51]. In this way, values less than 100% would indicate that the immobilization process would affect the catalytic capacity of the enzyme, while at higher values we would be in the presence of enzyme activation. The surface plot represented in **Figure 1F** shows a marked increase at 150 mM and pH 4. As can be seen in these conditions **RA** was slightly lower than 2000% reflecting a clear hyperactivation of the enzyme. In the rest of the conditions, **RA** showed values close to 100%, registering the lower ones when the immobilization was carried out at pH 8. This behavior suggested an enzymatic inactivation process probably due to conformational changes in the tertiary structure of the enzyme that compromised its catalytic capacity [52]. The statistical parameters of the design showed that both factors studied were significant in the response ($p < 0.05$; **Table 1**) with positive statistical effects for the ionic strength ($E = 124.15$) and

negative for the pH (E = -337,71). Thus, the proximity to the isoelectric point of the lipase was crucial for the occurrence of interfacial activation while variations in ionic strength towards higher values would reinforce the hydrophobic protein-support interaction leading to hyperactivation.

3.2. Surface charge

Z potential studies were carried out to determine the net surface charge in the different systems evaluated (**Figure 3A**). In terms of lipase surface charge, it exhibited typical behaviour around its isoelectric point, regardless of ionic strength, with positive values at pH 3 and 4, and negative values at pHs greater than 5. On the other hand, at 50 mM, $MgFe_2O_4$ exhibited a net negative charge or near neutrality throughout the pH range tested. This is due to the negatively charged external hydroxyl groups that are closely associated with the surface of this oxide and that come from the hydration water of the reaction medium. [53]. When we compare these results at 50 mM to those in **Figure 1A**, we can observe that larger **IP** recordings were obtained at acidic pH, which gradually decreases as the pH increases. As can also be seen in **Figure 3A**, the enzyme was positively charged (close to neutrality) at pH 3 and 4 and might interact electrostatically with $MgFe_2O_4$. When the systems were evaluated at 150 mM, the **IP** peak was observed between pH 5 and 6 (**Figure 1A**). Analyzing the surface charge of the oxide revealed that, like lipase, it acquires positive values at pH 3 and 4, which means that electrostatic repulsion may occur. Already at pH 5, the oxide got a negative charge close to 0, implying that it would obtain a neutral charge between pH 4 and 5, very near to the enzyme's isoelectric point. At pHs higher than 6 the net surface charge of the oxide and CRL was negative at both ionic strengths, therefore it is probable that electrostatic repulsion phenomena occur hindering CRL adsorption. The surface charges of the oxide after enzyme adsorption were more positive at pH 3 and 4 and more negative at pH 5. This could be associated with additional charges provided by the enzyme. The most negative values were recorded at 50 mM compared to those at 150 mM probably due to the lower amount of counterions present at low ionic strengths to neutralize the negative surface charges contributed by the protein.

3.3. Stability studies

The stability tests and subsequent analysis were conducted using the biocatalyst produced (CRLa@$MgFe_2O_4$) under the CCD model's settings, which maximized the amount of immobilized protein (pH 3.5 and ionic strength of 74.09 mM; **Table 2**). First of all, **Figure 3B** showed that CRLa@$MgFe_2O_4$ was more stable than the free enzyme at a temperature range of 30-50ºC. However, at 60ºC, a drop in the residual activity was observed, which was almost null at 80ºC. Similar behavior was observed by Zhuang et al. [54], who reported that a lipase immobilized on functionalized graphene oxide was less stable than the free one from 60ºC. This increase in stability and temperatures up to 50ºC lies in the conformational rigidity obtained by the enzyme after its immobilization increasing the energy needed to induce its denaturation [55]. Regarding pH stability (**Figure 3C**) the best values of residual activity were recorded at acidic pH, showing CRLa@$MgFe_2O_4$ considerably more stable than free CRL. This may be directly related to immobilization conditions. Nevertheless, when moving to higher pH, the residual activity fell slightly, possibly due to a progressive change of the microenvironment that would induce conformational changes in the enzyme, altering the protein-support interaction and leading to leakage problems.

Regarding organic solvent tolerance, the methanol strongly compromised the stability of CRLa@$MgFe_2O_4$ (**Figure 3D**), unlike free CRL which keeps up about 50% of activity. A similar effect was observed in the presence of butanol. On the other hand, good residual activities were measured in the presence of ethanol, propanol, and acetone compared to the free enzyme, registering values greater than or near 50% for CRLa@$MgFe_2O_4$. Since short-chain alcohols, such as ethanol, are frequently utilized in transesterification reactions, resistance to them is crucial [44,56]. The improved lipase stability may be attributed to the creation of a nano environment close to the support, which would prevent the denaturation of the enzyme. Therefore, the effective concentration of organic solvents in the enzyme's immediate vicinity is much lower than the concentration of the bulk solution [57,58]. According to the literature, those enzymes bound by hydrophobic interactions tend to be considered sensitive to environmental disruptions. The presence of electrostatic interactions would allow firmer adsorption of the enzyme, improving its conformational rigidity by a multipoint union and increasing its stability [59,60].

3.4. Spectroscopical analysis

3.3.1. Fourier transform infrared spectroscopy

The FT-IR spectra for $MgFe_2O_4$, CRL, and CRLa@$MgFe_2O_4$ are shown in **Figure 4A**. Characteristic peaks for CRL were observed at 1651 and 1537 cm^{-1} and correspond to the Amide I and II bands respectively [61]. The intensity of those peaks underwent changes after the immobilization of the enzyme indicating a conformational change that occurred at the level of the tertiary structure of the protein [49]. On the other hand, was possible to observe the characteristic peak of the hydroxyl groups near 3421 cm^{-1}, observing a slight shift towards values of 3222 cm^{-1}, suggesting the formation of hydrogen bonds during the immobilization process [30,62].

3.3.2. Raman spectroscopy

Figure 4B shows the Raman spectra for the different systems studied. The intense peak observed for the $MgFe_2O_4$ oxide at 690 cm^{-1} together with the weak band at 539 cm^{-1}, and 466, 311, and 208 cm^{-1} can be attributed to A_{1g}, E_g, F_{2g}, belonging to the motion of the oxygen atoms in tetrahedral AO_4 and octahedral BO_6 groups, respectively [63]. All signals are in agreement with the vibrational modes previously reported by other works [64].

The most important information derived from the analysis of a protein Raman spectrum lies in the vibrational modes associated with the amide groups and aromatic amino acids [65]. For the CRL spectrum, we can observe that the band of Amide I was located at 1650 cm^{-1} while that of Amide III was at 1328 cm^{-1}. After immobilizing the enzyme in both instances, a small spectral shift was noticed at higher wavelengths [66].

Concerning the aromatic amino acids, CRL presents in its structure 5 Trp, 20 Tyr, and 31 Phe [28]. First, Trp residues showed an intense band at 1557 cm^{-1} due to the indole ring, which is associated with a Fermi resonance that manifested as a doublet at 1360 and 1340 cm^{-1}. The intensity ratio recorded at both wavelengths (I_{1360}/I_{1340}) gives an idea of the hydrophobicity of the environment surrounding indole moieties [67]. In our work, the I_{1360}/I_{1340} was 0.8 for CRL, while it increased to 0.9 for the CRLa@$MgFe_2O_4$, which would indicate that there was an increase in hydrophobicity in the Trp environment.

The peak of maximum intensity at 1557 cm^{-1} corresponded to tyrosine (Tyr) residues and did not suffer shifts after the immobilization process. On the other hand, Tyr residues

are characterized by two specific bands of weak to medium intensity around 850 and 830 cm^{-1} and their intensity radio at these wavelengths (I_{850}/I_{830}) is indicative of the state of hydrogen bonds associated with the OH of the ring [68]. In our work, the free enzyme showed these peaks at 854 and 838 cm^{-1} with an I_{854}/I_{838} of 0.76 for CRL, while in the immobilized lipase, this value was modified to 0.66, which could indicate that phenolic OH in Tyr in CRL tend to act as a hydrogen-bond donor when interacted with $MgFe_2O_4$.

The phenylalanine residues in CRL showed one of the most intense bands in the spectrum at 1034 cm^{-1}, which is associated with a characteristic vibrational mode of the Phe aromatic ring [69]. The Raman intensity for this peak was significantly reduced when the spectrum of CRLa@$MgFe_2O_4$ was analyzed. This could suggest that the lipase adsorption would be restricting the ability of these amino acids to emit a signal in the spectrum, probably because they are strongly involved in the protein support interaction.

Another alteration observed in CRL after its immobilization was the shift of an intense band at 710 cm^{-1} towards 702 cm^{-1}, which is associated with the asymmetric stretching of the C-S bond in the Cys residues, possibly due to a disulfide bond breaking. In this sense, studies carried out with the lipase from *Thermomyces lanuginosus* suggested that the isomerization of disulfide bridges between Cys residues would be a key structural factor for the conformational transition of the enzyme between its open and closed form [65,70]. In this sense, the bands between 500 and 540 cm^{-1} associated with these bonds were analyzed before and after the immobilization process. CRL showed a medium-intensity single band at 523 cm^{-1} characteristics of the *trans-gauche-gauche* rotamers of the C-CH_2-S-S-CH_2-C fragment. However, CRLa@$MgFe_2O_4$ showed a dramatic conformational change around one of the S-S bridges to *trans-gauche-trans*, because of the appearance of a weak peak at 540 cm^{-1} attributed to the frequency ν(S-S) fragment.

3.5. *Molecular docking studies*

Molecular docking analysis was performed to theoretically observe (*in silico*) the interaction between $MgFe_2O_4$ and the CRL. **Figure 5A** shows the most likely binding point between a $MgFe_2O_4$ oxide in the lipase structure. As can be seen, the mesh of the oxide was located in the vicinity of the pocket and the lid, a region containing a catalytic triad that constitutes the active site of this enzyme. This could suggest that this protein-support

binding site could induce a conformational shift towards the open form of lipase, with the oxide binding in the vicinity of the lid and preventing its closure. **Figure 5B** also shows the interaction models produced by the molecular docking program where it was possible to observe the amino acids of the CRL that are involved in the interaction with the support, which is also listed in **Table 3**. The residues involved were mainly nonpolar, suggesting that hydrophobic-type interactions prevail in lipase adsorption. Four phenylalanine residues (Phe133, Phe296, Phe344, Phe448) and other nonpolar as Leu78, Leu297, or Ile453 were implicated in protein-support linkage. As seen earlier, the Raman intensity generated by Phe residues was markedly reduced after the immobilization. Moreover, we can also observe that protein-support interaction was also mediated through hydrogen bonds so that the generated hydrophobic interactions would be reinforced by others of an electrostatic nature that would involve Thr132 and Thr347 residues.

4. Conclusions

A precise balance of electrostatic and hydrophobic interactions can mediate lipase adsorption on solid supports. With the right fine-tuning, the immobilized enzyme could have high catalytic activity. In this regard, it was possible to optimize the immobilization of CRL on $MgFe_2O_4$ at pH 4, with an ionic strength of 90 mM; however, these immobilization conditions did not reflect the best **HA** in the CRLa@$MgFe_2O_4$, which was better to a higher ionic strength. Furthermore, strong interfacial hyperactivation was also observed in this last condition. This behaviour could be caused by surface hydrophobic protein-carrier interactions with aromatic amino acids like phenylalanine. Also, the contribution of interactions of an electrostatic nature at acidic pH contributed to the development of a multi-point attachment. Therefore, to obtain an active biocatalyst, it is necessary to understand the variables that influence the lipase immobilization process consider not only the enzyme and support nature but also the environment where the immobilization takes place. This work contributes to the understanding required for the suitable development of biocatalysts that might be exploited in biotechnologically relevant chemical reactions.

5. Acknowledgments

This work was supported by the Consejo Nacional de Investigaciones Científicas y Técnicas (PIP 0845), the Agencia Nacional de Promoción Científica y Tecnológica (PICT 2018–04448 and 2019-00742), and Universidad Nacional de Tucumán (PIUNT 26 D-616). A.L. thanks the Dr. Jorge Gomez Rojas of INBIONATEC-UNSE-CONICET, by the recorder to Raman spectra.

Figure Captions

Figure 1. Surface plots for the interaction between ionic strength and pH and its effect in CRL adsorption on $MgFe_2O_4$ for the design response: immobilized protein (**A**), hydrolytic activity (**B**), specific activity (**C**), Gibbs free energy (**D**), immobilized yield (**E**) and recovery activity (**F**).

Figure 2. Protein (**A**) and activity (**B**) isotherms for the immobilization of CRL on $MgFe_2O_4$ under the conditions generated by the CCD to maximize **IP** (**1**) or **HA** (**2**). The solid red line and the dashed blue line represent the fit of the experimental data to the equations of the Langmuir and Freundlich isotherms, respectively. q_t and k_t denote the amount of protein adsorbed and activity registered at the support at equilibrium, respectively, whilst C_e and A_e represent the residual protein and activity in solution after immobilization.

Figure 3. A. Z potential measurements for the $MgFe_2O_4$ without and with CRL adsorbed at 50 and 150 mM; MNPs = magnetic nanoparticles. Thermal (**B**), pH (**C**), and organic solvents (**C**) stabilities for free CRL and CRLa@$MgFe_2O_4$. The asterisk indicates that there were no significant differences between the pairs of trials compared.

Figure 4. Infrared (**A**) and Raman (**B**) spectra for $MgFe_2O_4$, CRL, and CRLa@$MgFe_2O_4$.

Figure 5. A. Most probable molecular docking model between CRL and $MgFe_2O_4$ oxide. The oxide mesh is represented by green and red spheres. **B.** Region of interaction between CRL and $MgFe_2O_4$ detailing the amino acids involved.

References

[1] P. Zucca, E. Sanjust, Inorganic Materials as Supports for Covalent Enzyme Immobilization: Methods and Mechanisms, (2014) 14139–14194. https://doi.org/10.3390/molecules190914139.

[2] T. Jesionowski, J. Zdarta, B. Krajewska, Enzyme immobilization by adsorption: a review, Adsorption. 20 (2014) 801–821. https://doi.org/10.1007/s10450-014-9623-y.

[3] M. Hoarau, S. Badieyan, E.N.G. Marsh, Immobilized enzymes: Understanding enzyme-surface interactions at the molecular level, Org Biomol Chem. 15 (2017) 9539–9551. https://doi.org/10.1039/c7ob01880k.

[4] M.G. Holyavka, S.S. Goncharova, A. v. Sorokin, M.S. Lavlinskaya, Y.A. Redko, D.A. Faizullin, D.R. Baidamshina, Y.F. Zuev, M.S. Kondratyev, A.R. Kayumov, V.G. Artyukhov, Novel Biocatalysts Based on Bromelain Immobilized on Functionalized Chitosans and Research on Their Structural Features, Polymers (Basel). 14 (2022). https://doi.org/10.3390/polym14235110.

[5] U. BORNSCHEUER, O. REIF, R. LAUSCH, R. FREITAG, T. SCHEPER, T. KOLISIS, U. MENGE, Lipase of Pseudomonas cepacia for biotechnological purposes: purification, crystallization and characterization, Biochimica et Biophysica Acta (BBA) - General Subjects. 1201 (1994) 55–60. https://doi.org/10.1016/0304-4165(94)90151-1.

[6] K. Dopierała, A. Kołodziejczak-Radzimska, K. Prochaska, T. Jesionowski, Immobilization of lipase in Langmuir − Blogett film of cubic silsesquioxane on the surface of zirconium dioxide, Appl Surf Sci. 573 (2022). https://doi.org/10.1016/j.apsusc.2021.151184.

[7] P. Reis, K. Holmberg, H. Watzke, M.E. Leser, R. Miller, Lipases at interfaces: A review, Adv Colloid Interface Sci. 147–148 (2009) 237–250. https://doi.org/10.1016/j.cis.2008.06.001.

[8] S. Arana-Peña, N.S. Rios, D. Carballares, L.R.B. Gonçalves, R. Fernandez-Lafuente, Immobilization of lipases via interfacial activation on hydrophobic supports: Production of biocatalysts libraries by altering the immobilization conditions, Catal Today. 362 (2021) 130–140. https://doi.org/10.1016/j.cattod.2020.03.059.

[9] J.M.F. Silva, K.P. dos Santos, E.S. dos Santos, N.S. Rios, L.R.B. Gonçalves, Immobilization of Thermomyces lanuginosus lipase on a new hydrophobic support (Streamline phenyl™): Strategies to improve stability and reusability, Enzyme Microb Technol. 163 (2023) 110166. https://doi.org/10.1016/j.enzmictec.2022.110166.

[10] R.C. Rodrigues, J.J. Virgen-Ortíz, J.C.S. dos Santos, Á. Berenguer-Murcia, A.R. Alcantara, O. Barbosa, C. Ortiz, R. Fernandez-Lafuente, Immobilization of lipases on hydrophobic supports: immobilization mechanism, advantages, problems, and solutions, Biotechnol Adv. 37 (2019) 746–770. https://doi.org/10.1016/j.biotechadv.2019.04.003.

[11] E.A. Manoel, J.C.S. dos Santos, D.M.G. Freire, N. Rueda, R. Fernandez-Lafuente, Immobilization of lipases on hydrophobic supports involves the open form of the enzyme, Enzyme Microb Technol. 71 (2015) 53–57. https://doi.org/10.1016/j.enzmictec.2015.02.001.

[12] W. Shuai, R.K. Das, M. Naghdi, S.K. Brar, M. Verma, A review on the important aspects of lipase immobilization on nanomaterials, Biotechnol Appl Biochem. 64 (2017) 496–508. https://doi.org/10.1002/bab.1515.

[13] H. Li, T. Wang, C. Su, J. Wu, P. van der Meeren, Effect of ionic strength on the sequential adsorption of whey proteins and low methoxy pectin on a hydrophobic surface: A QCM-D study, Food Hydrocoll. 122 (2022). https://doi.org/10.1016/j.foodhyd.2021.107074.

[14] J. Chen, Y. Sun, Modeling of the salt effects on hydrophobic adsorption equilibrium of protein, J Chromatogr A. 992 (2003) 29–40. https://doi.org/10.1016/S0021-9673(03)00277-2.

[15] K. Markandan, W.S. Chai, Perspectives on Nanomaterials and Nanotechnology for Sustainable Bioenergy Generation, Materials. 15 (2022). https://doi.org/10.3390/ma15217769.

[16] N.B. Machado, J.P. Miguez, I.C.A. Bolina, A.B. Salviano, R.A.B. Gomes, O.L. Tavano, J.H.H. Luiz, P.W. Tardioli, É.C. Cren, A.A. Mendes, Preparation, functionalization and characterization of rice husk silica for lipase immobilization via adsorption, Enzyme Microb Technol. 128 (2019) 9–21. https://doi.org/10.1016/j.enzmictec.2019.05.001.

[17] E. Parandi, M. Safaripour, M.H. Abdellattif, M. Saidi, A. Bozorgian, H. Rashidi Nodeh, S. Rezania, Biodiesel production from waste cooking oil using a novel biocatalyst of lipase enzyme immobilized magnetic nanocomposite, Fuel. 313 (2022) 123057. https://doi.org/10.1016/j.fuel.2021.123057.

[18] F. Esmi, T. Nematian, Z. Salehi, A.A. Khodadadi, A.K. Dalai, Amine and aldehyde functionalized mesoporous silica on magnetic nanoparticles for enhanced lipase immobilization, biodiesel production, and facile separation, Fuel. 291 (2021) 120126. https://doi.org/10.1016/j.fuel.2021.120126.

[19] S. Saire-Saire, S. Garcia-Segura, C. Tuyo, L.H. Andrade, H. Alarcon, Magnetic bio-nanocomposite catalysts of CoFe2O4/hydroxyapatite-lipase for enantioselective synthesis provide a framework for enzyme recovery and reuse, Int J Biol Macromol. 148 (2020) 284–291. https://doi.org/10.1016/j.ijbiomac.2020.01.137.

[20] M. Henrique da Silva Cavalcanti, L. Bueno Alves, A. Duarte, A. Aguiar Mendes, J. Maurício Schneedorf Ferreira da Silva, N. José Freitas da Silveira, M. Tsuyama Escote, L. Sindra Virtuoso, Immobilization of Thermomyces lanuginosus lipase via ionic adsorption on superparamagnetic iron oxide nanoparticles: Facile synthesis and improved catalytic performance, Chemical Engineering Journal. 431 (2022). https://doi.org/10.1016/j.cej.2021.134128.

[21] T. Carvalho, A. da S. Pereira, R.C.F. Bonomo, M. Franco, P. V. Finotelli, P.F.F. Amaral, Simple physical adsorption technique to immobilize Yarrowia lipolytica lipase purified by different methods on magnetic nanoparticles: Adsorption isotherms and thermodynamic approach, Int J Biol Macromol. 160 (2020) 889–902. https://doi.org/10.1016/j.ijbiomac.2020.05.174.

[22] C.M. Romero, F.C. Spuches, A.H. Morales, N.I. Perotti, M.C. Navarro, M.I. Gómez, Design and characterization of immobilized biocatalyst with lipase activity onto magnetic magnesium spinel nanoparticles: A novel platform for biocatalysis, Colloids Surf B Biointerfaces. 172 (2018) 699–707. https://doi.org/10.1016/j.colsurfb.2018.08.071.

[23] A.H. Morales, A.F. Alanís, G.S. Jaime, D.L. Lamas, M.I. Gómez, M.A. Martínez, C.M. Romero, Blend of renewable bio-based polymers for oil encapsulation: Control of the emulsion stability and scaffolds of the microcapsule by the gummy exudate of Prosopis nigra, Eur Polym J. 140 (2020) 109991. https://doi.org/10.1016/j.eurpolymj.2020.109991.

[24] M.B. Abdulhamid, J.S. Hero, M. Zamora, M.I. Gómez, M.C. Navarro, C.M. Romero, Effect of the biological functionalization of nanoparticles on magnetic CLEA preparation, Int J Biol Macromol. 191 (2021) 689–698. https://doi.org/10.1016/j.ijbiomac.2021.09.091.

[25] M.I. Gómez, G. Lucotti, J.A. De Morán, P.J. Aymonino, S. Pagola, P. Stephens, R.E. Carbonio, Ab initio structure solution of BaFeO2.8-δ, a new polytype in the system BaFeOy (2.5 ≤ y ≤ 3.0) prepared from the oxidative thermal decomposition of BaFe[(CN)5No] · 3H2O, J Solid State Chem. 160 (2001) 17–24. https://doi.org/10.1006/jssc.2001.9119.

[26] U.K. Winkler, M. Stuckmann, Glycogen , Hyaluronate , and Some Other Polysaccharides Greatly Enhance the Formation of Exolipase by Serratia marcescenst, 138 (1979) 663–670.

[27] M.M. Bradford, A Rapid and Sensitive Method for the Quantitation Microgram Quantities of Protein Utilizing the Principle of Protein-Dye Binding, 254 (1976) 248–254.

[28] P. Grochulski, Y. Li, J.D. Schrag, F. Bouthillier, P. Smith, D. Harrison, B. Rubin, M. Cygler, Insights into interfacial activation from an open structure of Candida rugosa lipase, Journal of Biological Chemistry. 268 (1993) 12843–12847. https://doi.org/10.1016/S0021-9258(18)31464-9.

[29] E.F. Pettersen, T.D. Goddard, C.C. Huang, G.S. Couch, D.M. Greenblatt, E.C. Meng, T.E. Ferrin, UCSF Chimera?A visualization system for exploratory research and analysis, J Comput Chem. 25 (2004) 1605–1612. https://doi.org/10.1002/jcc.20084.

[30] W. Zhuang, X. Quan, Z. Wang, W. Zhou, P. Yang, L. Ge, B. Villacorta Hernandez, J. Wu, M. Li, J. Zhou, C. Zhu, H. Ying, Interfacial microenvironment for lipase immobilization: Regulating the heterogeneity of graphene oxide, Chemical Engineering Journal. 394 (2020). https://doi.org/10.1016/j.cej.2020.125038.

[31] J. Meissner, A. Prause, B. Bharti, G.H. Findenegg, Characterization of protein adsorption onto silica nanoparticles: influence of pH and ionic strength, Colloid Polym Sci. 293 (2015) 3381–3391. https://doi.org/10.1007/s00396-015-3754-x.

[32] M. Collu, C. Carucci, A. Salis, Specific Anion Effects on Lipase Adsorption and Enzymatic Synthesis of Biodiesel in Nonaqueous Media, Langmuir. 36 (2020) 9465–9471. https://doi.org/10.1021/acs.langmuir.0c01330.

[33] S. Jakovetić Tanasković, B. Jokić, S. Grbavčić, I. Drvenica, N. Prlainović, N. Luković, Z. Knežević-Jugović, Immobilization of Candida antarctica lipase B on kaolin and its application in synthesis of lipophilic antioxidants, Appl Clay Sci. 135 (2017) 103–111. https://doi.org/10.1016/j.clay.2016.09.011.

[34] N.S. Okura, G.J. Sabi, M.C. Crivellenti, R.A.B. Gomes, R. Fernandez-Lafuente, A.A. Mendes, Improved immobilization of lipase from Thermomyces lanuginosus on a new chitosan-

based heterofunctional support: Mixed ion exchange plus hydrophobic interactions, Int J Biol Macromol. 163 (2020) 550–561. https://doi.org/10.1016/j.ijbiomac.2020.07.021.

[35] R.C.F. Bonomo, L.A. Minim, J.S.R. Coimbra, R.C.I. Fontan, L.H. Mendes da Silva, V.P.R. Minim, Hydrophobic interaction adsorption of whey proteins: Effect of temperature and salt concentration and thermodynamic analysis, J Chromatogr B Analyt Technol Biomed Life Sci. 844 (2006) 6–14. https://doi.org/10.1016/j.jchromb.2006.06.021.

[36] N.Ž. Prlainović, D.I. Bezbradica, Z.D. Knežević-Jugović, S.I. Stevanović, M.L. Avramov Ivić, P.S. Uskoković, D.Ž. Mijin, Adsorption of lipase from Candida rugosa on multi walled carbon nanotubes, Journal of Industrial and Engineering Chemistry. 19 (2013) 279–285. https://doi.org/10.1016/j.jiec.2012.08.012.

[37] N. Binhayeeding, T. Yunu, N. Pichid, S. Klomklao, K. Sangkharak, Immobilisation of Candida rugosa lipase on polyhydroxybutyrate via a combination of adsorption and cross-linking agents to enhance acylglycerol production, Process Biochemistry. 95 (2020) 174–185. https://doi.org/10.1016/j.procbio.2020.02.007.

[38] S. Zhang, J. Shi, Q. Deng, M. Zheng, C. Wan, C. Zheng, J. Li, F. Huang, Preparation of Carriers Based on ZnO Nanoparticles Decorated on Graphene Oxide (GO) Nanosheets for Efficient Immobilization of Lipase from Candida rugosa, Molecules. 22 (2017). https://doi.org/10.3390/molecules22071203.

[39] R.S. Gama, I.C.A. Bolina, É.C. Cren, A.A. Mendes, A novel functionalized SiO2-based support prepared from biomass waste for lipase adsorption, Mater Chem Phys. 234 (2019) 146–150. https://doi.org/10.1016/j.matchemphys.2019.06.002.

[40] M.D. Alves, F.M. Aracri, É.C. Cren, A.A. Mendes, Isotherm, kinetic, mechanism and thermodynamic studies of adsorption of a microbial lipase on a mesoporous and hydrophobic resin, Chemical Engineering Journal. 311 (2017) 1–12. https://doi.org/10.1016/j.cej.2016.11.069.

[41] M. Sarno, M. Iuliano, Highly active and stable Fe3O4/Au nanoparticles supporting lipase catalyst for biodiesel production from waste tomato, Appl Surf Sci. 474 (2019) 135–146. https://doi.org/10.1016/j.apsusc.2018.04.060.

[42] I.C.A. Bolina, A.B. Salviano, P.W. Tardioli, É.C. Cren, A.A. Mendes, Preparation of ion-exchange supports via activation of epoxy-SiO2 with glycine to immobilize microbial lipase – Use of biocatalysts in hydrolysis and esterification reactions, Int J Biol Macromol. 120 (2018) 2354–2365. https://doi.org/10.1016/j.ijbiomac.2018.08.190.

[43] J.J. Virgen-Ortíz, V.G. Tacias-Pascacio, D.B. Hirata, B. Torrestiana-Sanchez, A. Rosales-Quintero, R. Fernandez-Lafuente, Relevance of substrates and products on the desorption of lipases physically adsorbed on hydrophobic supports, Enzyme Microb Technol. 96 (2017) 30–35. https://doi.org/10.1016/j.enzmictec.2016.09.010.

[44] I. Kurtovic, T.D. Nalder, H. Cleaver, S.N. Marshall, Immobilisation of Candida rugosa lipase on a highly hydrophobic support: A stable immobilised lipase suitable for non-aqueous synthesis, Biotechnology Reports. 28 (2020). https://doi.org/10.1016/j.btre.2020.e00535.

[45] M. Tu, X. Pan, J.N. Saddler, Adsorption of Cellulase on Cellulolytic Enzyme Lignin from Lodgepole Pine, J Agric Food Chem. 57 (2009) 7771–7778. https://doi.org/10.1021/jf901031m.

[46] F.A.P. Lage, J.J. Bassi, M.C.C. Corradini, L.M. Todero, J.H.H. Luiz, A.A. Mendes, Preparation of a biocatalyst via physical adsorption of lipase from Thermomyces lanuginosus on hydrophobic support to catalyze biolubricant synthesis by esterification reaction in a solvent-free system, Enzyme Microb Technol. 84 (2016) 56–67. https://doi.org/10.1016/j.enzmictec.2015.12.007.

[47] R.A. Latour, The Langmuir isotherm: A commonly applied but misleading approach for the analysis of protein adsorption behavior, J Biomed Mater Res A. 103 (2015) 949–958. https://doi.org/10.1002/jbm.a.35235.

[48] T. Carvalho, A. da S. Pereira, R.C.F. Bonomo, M. Franco, P. V. Finotelli, P.F.F. Amaral, Simple physical adsorption technique to immobilize Yarrowia lipolytica lipase purified by different methods on magnetic nanoparticles: Adsorption isotherms and thermodynamic approach, Int J Biol Macromol. 160 (2020) 889–902. https://doi.org/10.1016/j.ijbiomac.2020.05.174.

[49] N.S. Mohammadi, M.S. Khiabani, B. Ghanbarzadeh, R. R. Mokarram, Improvement of lipase biochemical properties via a two-step immobilization method: Adsorption onto silicon dioxide nanoparticles and entrapment in a polyvinyl alcohol/alginate hydrogel, J Biotechnol. 323 (2020) 189–202. https://doi.org/10.1016/j.jbiotec.2020.07.002.

[50] F. Nekouei, S. Nekouei, I. Tyagi, V.K. Gupta, Kinetic, thermodynamic and isotherm studies for acid blue 129 removal from liquids using copper oxide nanoparticle-modified activated carbon as a novel adsorbent, J Mol Liq. 201 (2015) 124–133. https://doi.org/10.1016/j.molliq.2014.09.027.

[51] L.N. Lima, G.C. Oliveira, M.J. Rojas, H.F. Castro, P.C.M. Da Rós, A.A. Mendes, R.L.C. Giordano, P.W. Tardioli, Immobilization of Pseudomonas fluorescens lipase on hydrophobic supports and application in biodiesel synthesis by transesterification of vegetable oils in solvent-free systems, J Ind Microbiol Biotechnol. 42 (2015) 523–535. https://doi.org/10.1007/s10295-015-1586-9.

[52] R.A. Sheldon, S. van Pelt, Enzyme immobilisation in biocatalysis: why, what and how, Chem. Soc. Rev. 42 (2013) 6223–6235. https://doi.org/10.1039/C3CS60075K.

[53] J. Feng, S. Yu, J. Li, T. Mo, P. Li, Enhancement of the catalytic activity and stability of immobilized aminoacylase using modified magnetic Fe3O4 nanoparticles, Chemical Engineering Journal. 286 (2016) 216–222. https://doi.org/10.1016/j.cej.2015.10.083.

[54] W. Zhuang, W. Gu, Q. Zhu, J. Zhu, Z. Wang, H. Niu, D. Liu, J. Wu, Y. Chen, M. Li, C. Zhu, H. Ying, Surface functionalization of graphene oxide by disodium guanosine 5'-monophosphate and its excellent performance for lipase immobilization, Appl Surf Sci. 492 (2019) 27–36. https://doi.org/10.1016/j.apsusc.2019.05.166.

[55] H. Aghaei, A. Yasinian, A. Taghizadeh, Covalent immobilization of lipase from Candida rugosa on epoxy-activated cloisite 30B as a new heterofunctional carrier and its application

in the synthesis of banana flavor and production of biodiesel, Int J Biol Macromol. 178 (2021) 569–579. https://doi.org/10.1016/j.ijbiomac.2021.02.146.

[56] S. Javed, F. Azeem, S. Hussain, I. Rasul, M.H. Siddique, M. Riaz, M. Afzal, A. Kouser, H. Nadeem, Bacterial lipases: A review on purification and characterization, Prog Biophys Mol Biol. 132 (2018) 23–34. https://doi.org/10.1016/j.pbiomolbio.2017.07.014.

[57] N.M. Mesbah, Covalent immobilization of a halophilic, alkalithermostable lipase LipR2 on Florisil ® nanoparticles for production of alkyl levulinates, Arch Biochem Biophys. 667 (2019) 22–29. https://doi.org/10.1016/j.abb.2019.04.004.

[58] A. Kumar, K. Dhar, S.S. Kanwar, P.K. Arora, Lipase catalysis in organic solvents: Advantages and applications, Biol Proced Online. 18 (2016). https://doi.org/10.1186/s12575-016-0033-2.

[59] A.H. Morales, J.S. Hero, M.C. Navarro, E.M. Farfán, M.A. Martínez, D.L. Lamas, M.I. Gómez, C.M. Romero, Design of an Immobilized Biohybrid Catalyst by Adsorption Interactions onto Magnetic Srebrodolskite Nanoparticles, ChemistrySelect. 4 (2019) 11024–11033. https://doi.org/10.1002/slct.201903306.

[60] A.M. Girelli, V. Chiappini, P. Amadoro, Immobilization of lipase on spent coffee grounds by physical and covalent methods: A comparison study, Biochem Eng J. 192 (2023) 108827. https://doi.org/10.1016/j.bej.2023.108827.

[61] M. Sarno, M. Iuliano, G_Fe3O4/Ag supporting Candida rugosa lipase for the “green” synthesis of pomegranate seed oil derived liquid wax esters, Appl Surf Sci. 510 (2020). https://doi.org/10.1016/j.apsusc.2020.145481.

[62] N.Ž. Prlainović, D.I. Bezbradica, A.D. Knežević-Jugović, S.I. Stevanović, M.L. Avramov Ivić, P.S. Uskoković, D.Ž. Mijin, Adsorption of lipase from Candida rugosa on multi walled carbon nanotubes, Journal of Industrial and Engineering Chemistry. 19 (2013) 279–285. https://doi.org/10.1016/j.jiec.2012.08.012.

[63] F. Naaz, H.K. Dubey, C. Kumari, P. Lahiri, Structural and magnetic properties of MgFe2O4 nanopowder synthesized via co-precipitation route, SN Appl Sci. 2 (2020) 808. https://doi.org/10.1007/s42452-020-2611-9.

[64] J. Chandradass, A.H. Jadhav, K.H. Kim, H. Kim, Influence of processing methodology on the structural and magnetic behavior of MgFe 2O 4 nanopowders, J Alloys Compd. 517 (2012) 164–169. https://doi.org/10.1016/j.jallcom.2011.12.071.

[65] A. Misiunas, Z. Talaikyte, G. Niaura, V. Razumas, T. Nylander, Thermomyces lanuginosus lipase in the liquid-crystalline phases of aqueous phytantriol: X-ray diffraction and vibrational spectroscopic studies, Biophys Chem. 134 (2008) 144–156. https://doi.org/10.1016/j.bpc.2008.02.002.

[66] A.E. Ledesma, D.M. Chemes, M. de los A. Frías, M. del P. Guauque Torres, Spectroscopic characterization and docking studies of ZnO nanoparticle modified with BSA, Appl Surf Sci. 412 (2017) 177–188. https://doi.org/10.1016/j.apsusc.2017.03.202.

[67] R. Žukiene, V. Snitka, Zinc oxide nanoparticle and bovine serum albumin interaction and nanoparticles influence on cytotoxicity in vitro, Colloids Surf B Biointerfaces. 135 (2015) 316–323. https://doi.org/10.1016/j.colsurfb.2015.07.054.

[68] M.N. Siamwiza, R.C. Lord, M.C. Chen, T. Takamatsu, I. Harada, H. Matsuura, T. Shimanoxhi, Interpretation of the Doublet at 850 and 830 cm-l in the Raman Spectra of Tyrosyl Residues in Proteins and Certain Model Compoundsi, n.d.

[69] B. Sjöberg, S. Foley, B. Cardey, M. Enescu, An experimental and theoretical study of the amino acid side chain Raman bands in proteins, Spectrochim Acta A Mol Biomol Spectrosc. 128 (2014) 300–311. https://doi.org/10.1016/j.saa.2014.02.080.

[70] A.M. Brzozowski, H. Savage, C.S. Verma, J.P. Turkenburg, D.M. Lawson, A. Svendsen, S. Patkar, Structural origins of the interfacial activation in Thermomyces (Humicola) lanuginosa lipase, Biochemistry. 39 (2000) 15071–15082. https://doi.org/10.1021/bi0013905.

Table 1. Statistical parameters associated with the CCD for the immobilization of CRL onto $MgFe_2O_4$, taking as responses: immobilized protein (**IP**), hydrolytic activity (**HA**), specific activity (**SA**), Gibbs free energy (**ΔG**) immobilization yield (**IY**) and recovered activity (**RA**).

	IP		**HA**		**SA**		**ΔG**		**IY**		**RA**	
FACTORS	Effect	*p*-value	Effect	*p*-value	Effect	*p*-value	Effect	*p*-value	Effect	*p*-value	Effect	*p*-value
pH (A)	-0.9883	< 0.0001	-5.74	< 0.0001	11.61	< 0.0001	4.26	< 0.0001	-3.47	0.0038	-337.71	< 0.0001
Ionic Strength (B)	0.0869	0.1348	-1.09	0.0521	-0.9669	0.4645	0.2140	0.3903	-9.72	< 0.0001	124.15	0.0006
AB	-0.0027	0.9613	-1.51	0.0116	1.98	0.1487	0.2353	0.3466	4.79	0.0004	-39.32	< 0.0001
A^2	0.0892	0.1257	0.015	0.9976	5.52	0.0012	-0.5377	0.0461	27.78	< 0.0001	65.27	0.0299
B^2	0.2663	0.0004	-0.8601	0.1127	-2.35	0.0923	-0.7761	0.0078	3.36	0.0046	-16.56	0.5401
A^2B	-0.5381	< 0.0001	1.98	0.0172	7.68	0.0014	1.30	0.0027	1.17	0.4029	272.12	< 0.0001
AB^2	0.5932	< 0.0001	2.25	0.0087	-8.36	0.0007	-3.34	< 0.0001	9.25	< 0.0001	-125.26	0.0061
A^2B^2	-0.4555	< 0.0001	-1.94	0.0188	-1.02	0.5828	1.27	0.0031	12.71	< 0.0001	55.51	0.1620
Model	-	< 0.0001	-	< 0.0001	-	< 0.0001	-	< 0.0001	-	< 0.0001	-	< 0.0001

	01	01	01	01	01	01
$\mathbf{R^2}$	0.9790	0.9512	0.9357	0.9728	0.9934	0.9889
$\mathbf{R^2_{adjusted}}$	0.9637	0.9157	0.8889	0.9530	0.9885	0.9808

Table 2. Optimal conditions provided by the CCD to maximize the **IP** (mg protein/mg support) or **HA** (IU/mg support) responses during the immobilization of CRL on $MgFe_2O_4$. The expected values based on the model and those obtained experimentally are shown. The associated parameters for the adjustment of the experimental data to the protein and activity isotherms to the Langmuir and Freundlich models for both conditions are also detailed.

		Maximizing IP	**Maximizing HA**
CCD conditions	pH	3.25	3.00
	IS	74.09	114.203
Expected values	**IP**	3.249	2.852
	HA	28.830	34.949
	Desirability	0.816	0.930
Practical values	**IP**	3.53 ± 0.05	2.51 ± 0.09
	HA	31.11 ± 2.44	38.31 ± 1.23
Langmuir Model (protein isotherms)	q_{max}	3.888	3.197
	K_L	0.0693	0.2136
	R^2	0.8362	0.9569
Freundlich Model (protein isotherms)	n	6.327	4.053
	K_F	3.425	2.442
	R^2	0.6739	0.7942
Langmuir Model (activity isotherms)	q_{max}	72.38	75.96
	K_L	0.5120	1.237
	R^2	0.9345	0.9888
Freundlich Model (activity isotherms)	n	1.577	1.445
	K_F	52.92	33.73
	R^2	0.8998	0.9804

IS = Ionic strength (mM)

Table 3. Binding energy, inhibition constant, amino acid residues and the occurrence of hydrogen bonds involved in the interaction of CRL with the $MgFe_2O_4$ after performing the molecular docking.

Binding energy (kcal/mol)	-8.03
$K_{inhibition}$ (µM)	1.0
Amino acids involved	Pro65 Leu78 Leu297 Val 127 Gly128 Thr132 The347 Phe133 Phe296 Phe344 Phe448 Glu208 Ser450 Ile453
Hydrogen bonds	Thr132 Thr347

Author statement

Andrés H. Morales: Conceptualization, Methodology, Investigation, Formal Analysis, Writing – Original Draft; **Johan S. Hero:** Software, Investigation, Visualization **Ana E. Ledesma:** Software, Formal Analysis; **M. Alejandra Martínez:** Resources, Supervision; **María C. Navarro**: Resources, Visualization; **María I. Gómez:** Resources **Cintia M. Romero:** Conceptualization, Writing – Review and Editing, Supervision, Funding Acquisition.

Declaration of interests

☒ The authors declare that they have no known competing financial interests or personal relationships that could have appeared to influence the work reported in this paper.

☐The authors declare the following financial interests/personal relationships which may be considered as potential competing interests:

Graphical abstract

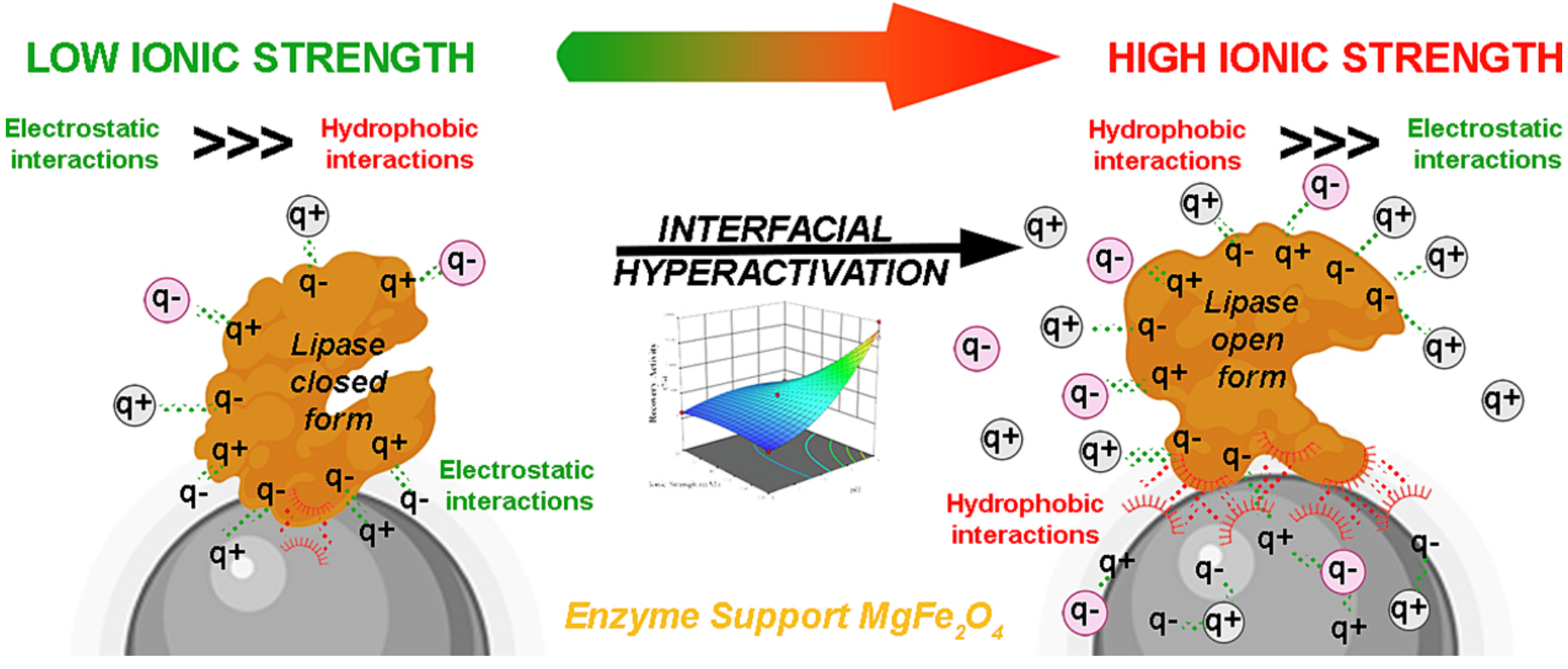

Graphics Abstract

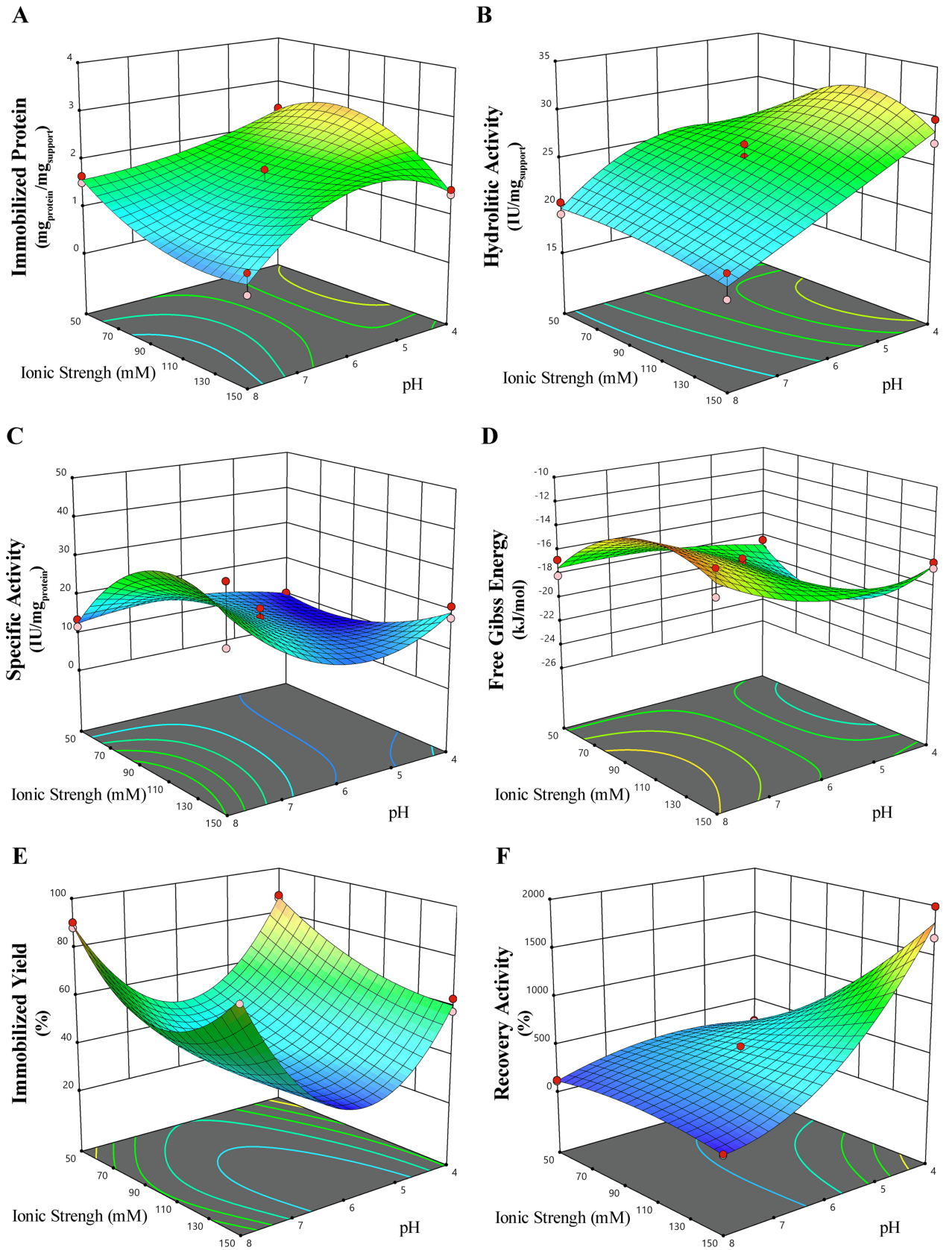
A
Immobilized Protein
(mg$_{protein}$/mg$_{support}$)
Ionic Strengh (mM)
pH
B
Hydrolitic Activity
(IU/mg$_{support}$)
Ionic Strengh (mM)
pH
C
Specific Activity
(IU/mg$_{protein}$)
Ionic Strengh (mM)
pH
D
Free Gibss Energy
(kJ/mol)
Ionic Strengh (mM)
pH
E
Immobilized Yield
(%)
Ionic Strengh (mM)
pH
F
Recovery Activity
(%)
Ionic Strengh (mM)
pH

Figure 1

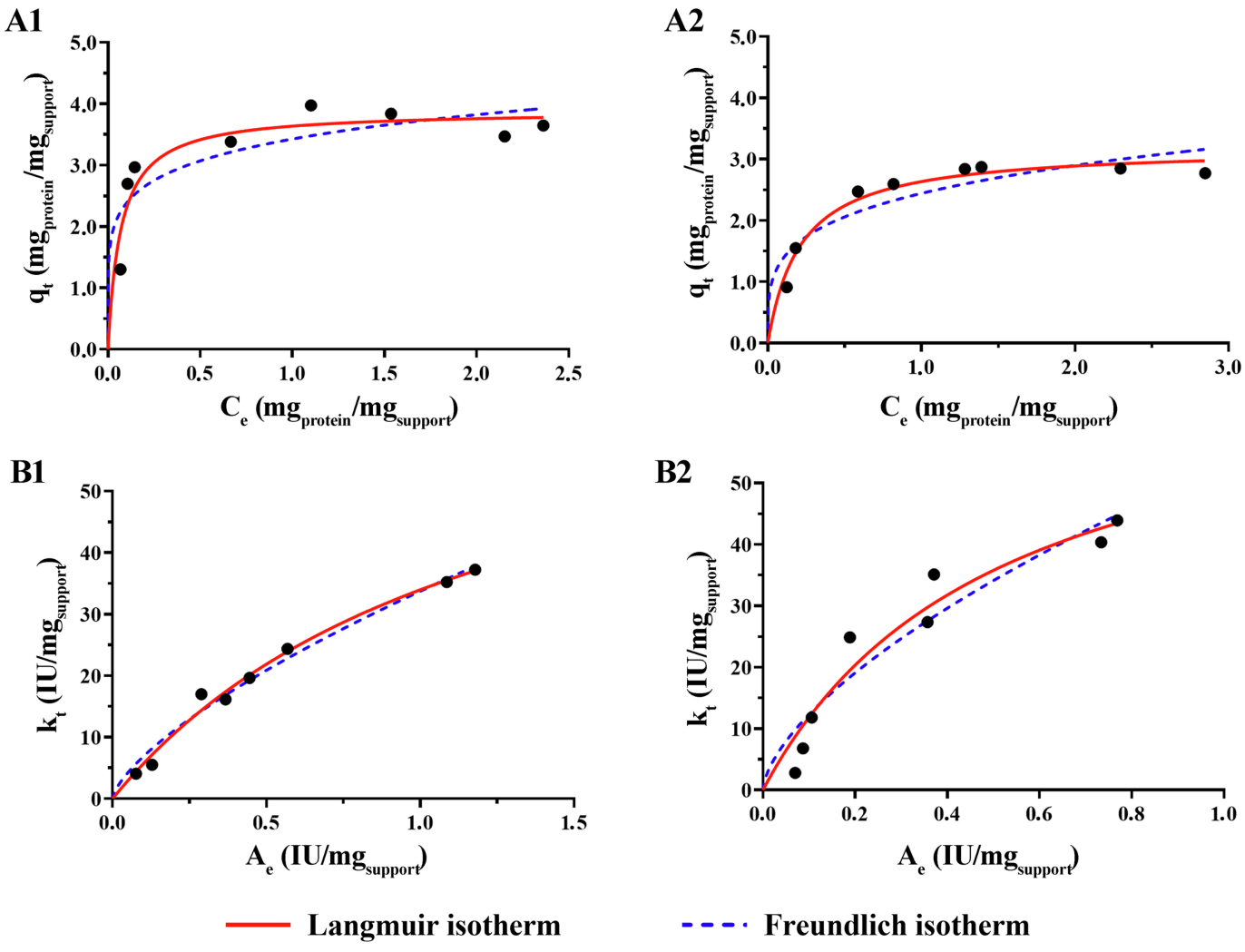
A1
A2
B1
B2
q_t ($mg_{protein}$/$mg_{support}$)
C_e ($mg_{protein}$/$mg_{support}$)
k_t (IU/$mg_{support}$)
A_e (IU/$mg_{support}$)
Langmuir isotherm
Freundlich isotherm

Figure 2

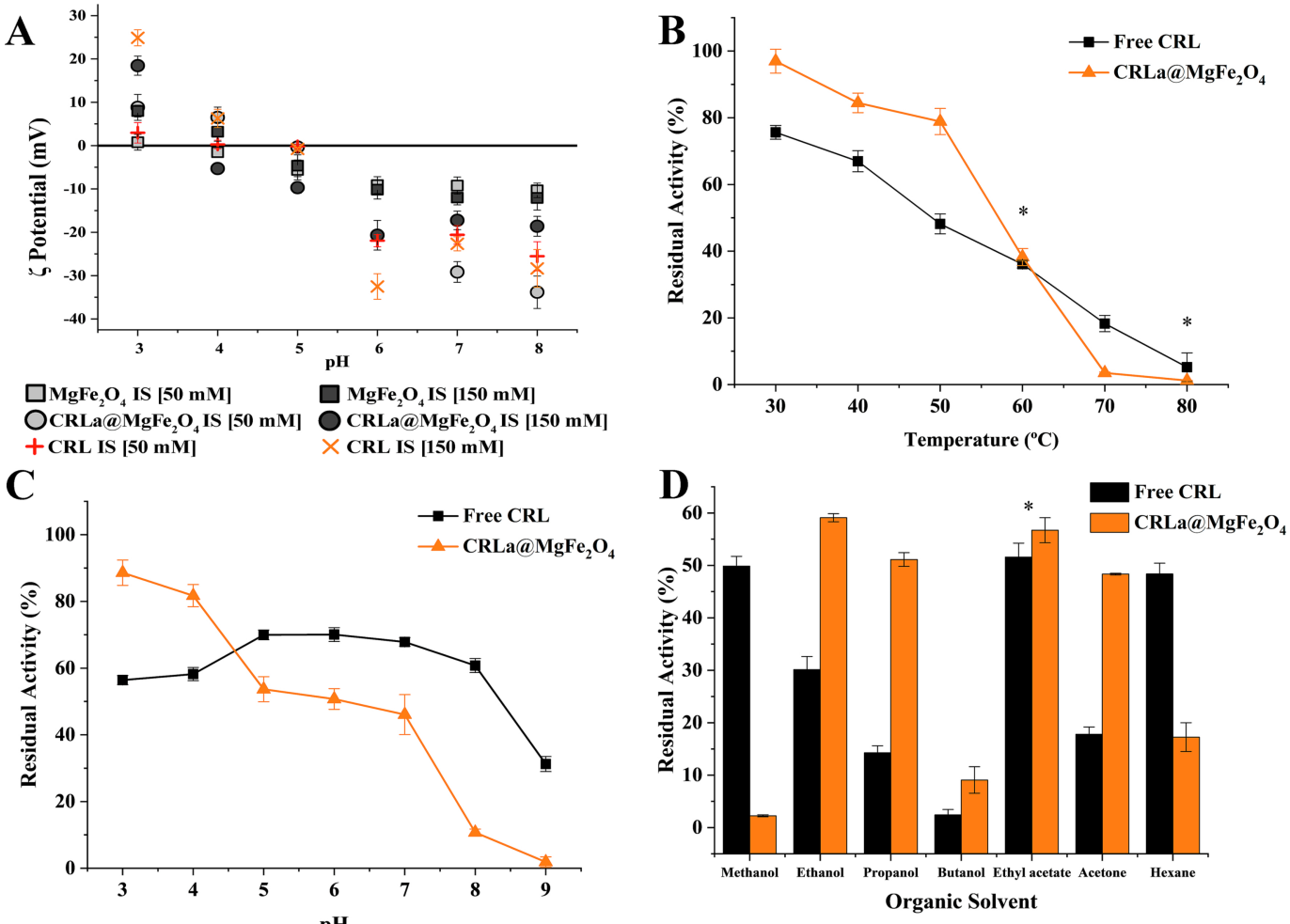
A
ζ Potential (mV)
pH
MgFe2O4 IS [50 mM]
MgFe2O4 IS [150 mM]
CRLa@MgFe2O4 IS [50 mM]
CRLa@MgFe2O4 IS [150 mM]
CRL IS [50 mM]
CRL IS [150 mM]
B
Residual Activity (%)
Temperature (°C)
Free CRL
CRLa@MgFe2O4
C
Residual Activity (%)
pH
Free CRL
CRLa@MgFe2O4
D
Residual Activity (%)
Organic Solvent
Free CRL
CRLa@MgFe2O4
Methanol
Ethanol
Propanol
Butanol
Ethyl acetate
Acetone
Hexane

Figure 3

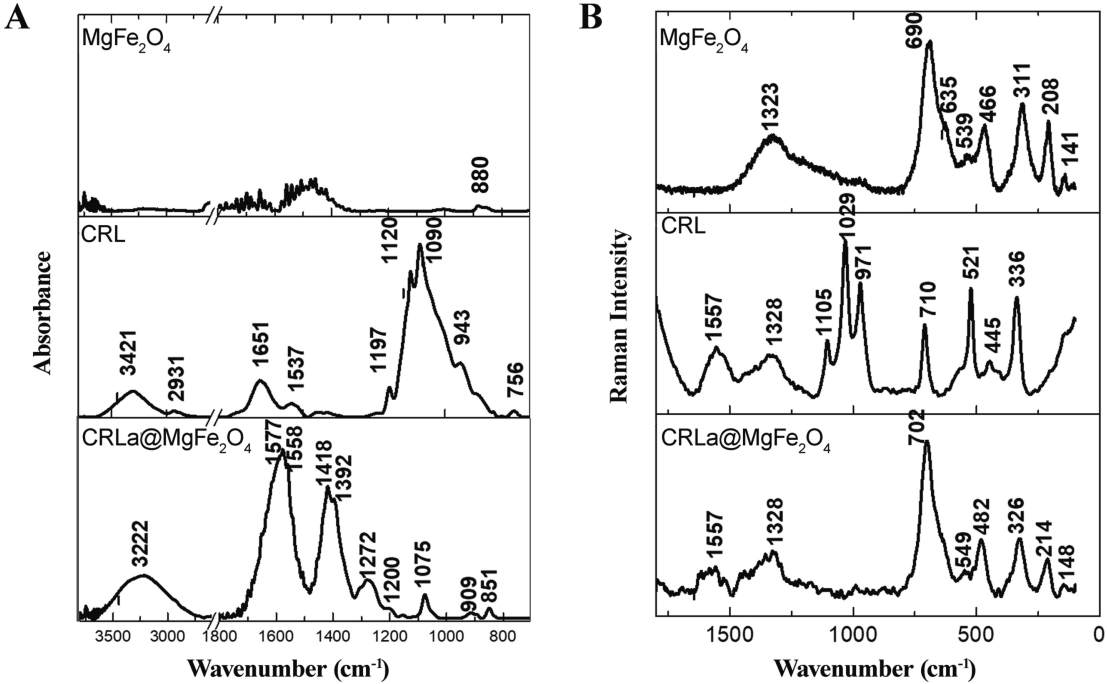
A
MgFe2O4
880
CRL
3421
2931
1651
1537
1197
1120
1090
943
756
CRLa@MgFe2O4
3222
1577
1558
1418
1392
1272
1200
1075
909
851
Absorbance
3500 3000 1800 1600 1400 1200 1000 800
Wavenumber (cm-1)
B
MgFe2O4
1323
690
635
539
466
311
208
141
CRL
1557
1328
1105
1029
971
710
521
445
336
CRLa@MgFe2O4
1557
1328
702
549
482
326
214
148
Raman Intensity
1500 1000 500 0
Wavenumber (cm-1)

Figure 4

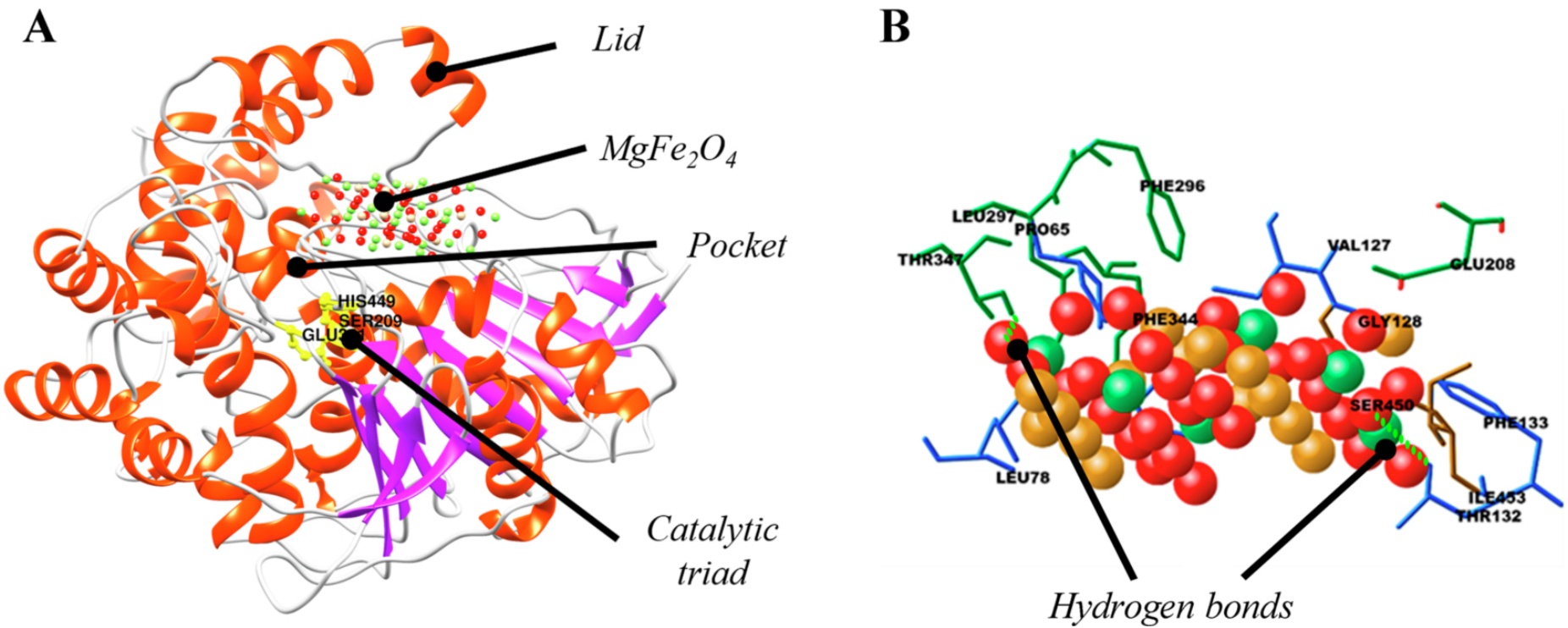
A
Lid
$MgFe_2O_4$
Pocket
HIS449
SER209
Catalytic
triad
B
PHE296
LEU297
PRO65
THR347
VAL127
GLU208
PHE344
GLY128
SER450
PHE133
LEU78
ILE453
THR132
Hydrogen bonds

Figure 5